NeuroImage 53 (2010) 1233–1243

Contents lists available at ScienceDirect

NeuroImage

journal homepage: www.elsevier.com/locate/ynimg

Track-density imaging (TDI): Super-resolution white matter imaging using whole-brain track-density mapping

Fernando Calamante *[,1], Jacques-Donald Tournier [1], Graeme D. Jackson, Alan Connelly

Brain Research Institute, Florey Neuroscience Institutes (Austin), Neurosciences Building, Banksia Street, Heidelberg West, Victoria 3081, Australia
Department of Medicine, University of Melbourne, Melbourne, Australia

ARTICLE INFO

Article history:
Received 23 April 2010
Revised 21 June 2010
Accepted 12 July 2010
Available online 17 July 2010

Keywords:
Magnetic resonance imaging
Super-resolution
White matter
Fiber-tracking
Diffusion MRI

ABSTRACT

Neuroimaging advances have given rise to major progress in neurosciences and neurology, as ever more subtle and specific imaging methods reveal new aspects of the brain. One major limitation of current methods is the spatial scale of the information available. We present an approach to gain spatial resolution using post-processing methods based on diffusion MRI fiber-tracking, to reveal structures beyond the resolution of the acquired imaging voxel; we term such a method as super-resolution *track-density imaging* (TDI). A major unmet challenge in imaging is the identification of abnormalities in white matter as a cause of illness; super-resolution TDI is shown to produce high-quality white matter images, with high spatial resolution and outstanding anatomical contrast. A unique property of these maps is demonstrated: their spatial resolution and signal-to-noise ratio can be tailored depending on the chosen image resolution and total number of fiber-tracks generated. Super-resolution TDI should greatly enhance the study of white matter in disorders of the brain and mind.

Introduction

The advent of neuroimaging has undoubtedly been one of the major contributors to advances in the neurosciences and clinical neurology. Each subsequent major advance in brain imaging, such as those in MRI of functional MRI (fMRI) for cognition (Kwong et al., 1992; Bandettini, 2009; Matthews et al., 2006) and diffusion-weighted imaging (DWI) for stroke (Moseley et al., 1990; Thomas et al., 2000), has been the precursor to new understanding of brain function and the basis of disease, as well as provided impetus for new clinical applications (Matthews et al., 2006; Gillard et al., 2005). Even though it can be argued that much of this knowledge was available from histopathological studies in post-mortem brains and from other techniques, advanced neuroimaging methods link *in vivo* the immediate clinical problem directly with the underlying brain structure and function in individual subjects. Many of the major advances in understanding the basis of brain abnormalities in disease have arisen from the ability to image the whole-brain and detect underlying pathology, with ever increasing sophistication. Importantly, each new neuroimaging technical advance has led to new insights, as ever more subtle and specific imaging and post-processing methods reveal new information about the brain that can be clinically applied.

One major limitation of current neuroimaging methods, compared to traditional histopathology, is the spatial scale of the information available. Many structures of biological interest are small compared to the scale of the imaging voxel. Increased signal-to-noise ratio (SNR) can allow improved spatial resolution to be achieved (i.e. smaller voxels), and is part of the impetus for ultra-high field MRI at 7 T and beyond (Duyn et al., 2007). Our proposed approach is to gain spatial resolution using post-processing methods, to reveal structures beyond the resolution of the acquired imaging voxel by using additional information obtained from outside that voxel. We propose such a super-resolution method (which we term as super-resolution *track-density imaging*, or super-resolution TDI) in the current study.

The aims of this study are to:

1. Propose a method to generate higher resolution (i.e. super-resolution) anatomical images with high anatomical contrast, by incorporating extra information from diffusion tractography modeling.
2. Demonstrate that these super-resolution images allow a *direct* visualization of important sub-structures of the functional nodes of the brain network (e.g. the thalamic nuclei and the cerebellar

Abbreviations: TDI, track-density imaging; CT, computed tomography; fMRI, functional MRI; DWI, diffusion-weighted imaging; SNR, signal-to-noise ratio; FA, fractional anisotropy; CNR, contrast-to-noise ratio; ROI, region of interest; SCP, superior cerebellar peduncles; MCP, middle cerebellar peduncles; ICP, inferior cerebellar peduncles; CSF, cerebrospinal fluid; HARDI, high angular resolution diffusion imaging; CSD, constrained spherical deconvolution; VBM, voxel-based morphometry; VBA, voxel-based analysis; SE–EPI, spin-echo echo-planar imaging; MPRAGE, magnetization-prepared rapid-acquisition with gradient-echo; TE, echo time; TR, repetition time; TI, inversion time.

* Corresponding author. Brain Research Institute, Neurosciences Building, Banksia Street, Heidelberg West, Victoria 3081, Australia. Fax: +61 3 9496 4071.
E-mail address: fercala@brain.org.au (F. Calamante).

[1] These authors contributed equally to this work.

1053-8119/$ – see front matter © 2010 Elsevier Inc. All rights reserved.
doi:10.1016/j.neuroimage.2010.07.024

peduncles) not easily identified on high-resolution conventional MRI.
3. Use the super-resolution images to demonstrate structural connections from the thalamus to the cortex, as well as the cerebellar sub-networks.

Such an advance in neuroimaging, which allows high-quality brain images to be generated at a resolution not feasible before with standard MRI technology, should have far reaching consequences on neuroscience.

Materials and methods

Data acquisition

DWI data were acquired from 5 healthy volunteers on a 3 T Siemens Trio system, using a twice-refocused SE–EPI sequence (Reese et al., 2003) ($b = 3000$ s/mm^2). Three subjects (subjects *S1–S3*) were scanned with 150 DWI-directions, 54 contiguous slices, voxel size $2.3 \times 2.3 \times 2.3$ mm^3, and acquisition time: 20.5 min. A further subject (*S4*) was scanned with 60 DWI-directions, 60 contiguous slices, voxel size $2.5 \times 2.5 \times 2.5$ mm^3, and acquisition time: 9.4 min. The final subject (*S5*) was scanned with 20 DWI-directions, 60 contiguous slices, voxel size $2.5 \times 2.5 \times 2.5$ mm^3, and acquisition time: 2.9 min. For all cases, a $b = 0$ volume was acquired first, and repeated after every 10 DWI-volumes. For each subject, a 3D high-resolution magnetization-prepared rapid-acquisition with gradient-echo (MPRAGE) data-set was also acquired for anatomical reference: voxel size $1 \times 1 \times 1$ mm^3, TE/TR/TI = 2.6/1900/900 ms, and flip-angle = 9°. Informed written consent was obtained from all subjects in accordance with ethical approval from the local Human Research Ethics Committee (Austin Health).

Fiber-tracking

Fiber-tracking was performed using the *MRtrix* software package (Brain Research Institute, Melbourne, Australia, http://www.brain.org.au/software/), based on the probabilistic streamlines method (Behrens et al., 2003; Parker and Alexander, 2005) combined with the constrained spherical deconvolution (CSD) technique (Tournier et al., 2007) to model multiple fiber-orientations. Tracking was performed by randomly seeding throughout the brain (for the 'whole-brain' tracking) or within the seed ROI (for 'targeted' tracking). The relevant fiber-tracking parameters were: 0.1 mm step-size, maximum angle between steps = 20°, any track with length <10 mm was discarded, termination criteria: exit the brain or when the CSD fiber-orientation distribution amplitude was <0.1. The primary parameter of interest in CSD is the maximum harmonic order l_{max} (which determines the 'sharpness' of the fiber-orientation distributions) (Tournier et al., 2007; Tournier et al., 2004); the value employed in this study depended on the total number of DWI-directions used to acquire the data: $l_{max} = 10/8/6$ for 150/60/20 DWI-directions, respectively.

Track-density imaging (TDI)

In order to generate the track-density maps, whole-brain probabilistic fiber-tracking was performed as an initial step (generated by randomly seeding a large number of tracks throughout the brain, e.g. 2,500,000 for Fig. 1 and Fig. 2). From these fiber-tracks, the total number of tracks present in each element of a grid was then calculated. It should be noted that the grid element can be *smaller* than the acquired voxel size, and therefore the resolution of the final map can be much higher than the source DWI data, i.e. super-resolution can be achieved by using the extra information provided by the (modeling) tractography results — e.g. see Figs. 1 and 2 for examples of 125 μm resolution. The proposed TDI method uses the continuity information contained in the streamlines to introduce sub-voxel information based on supporting information for each track from neighbouring voxels. Streamlines will therefore traverse a given voxel at a particular set of spatial locations within the voxel; when a sufficiently large number of streamlines have been created, their density can then be used as intra-voxel information to construct a super-resolution TDI image with higher spatial resolution than that of the source DWI data.

Grid resolution vs. number of tracks

To investigate the trade-off between the number of tracks required and image quality (for a given MRI protocol and grid-size in the final map), the correlation ρ between a 'reference' whole-brain track-density map (generated from a large number of tracks for a given grid-size) and the corresponding map generated with a subset n of the tracks was calculated:

$$\rho(n) = \frac{\mathrm{cov}(X_n, X_{ref})}{\sigma_{X_n} \cdot \sigma_{X_{ref}}} = \frac{E\left[\left(X_n - \mu_{X_n}\right) \cdot \left(X_{ref} - \mu_{X_{ref}}\right)\right]}{\sigma_{X_n} \cdot \sigma_{X_{ref}}} \quad (1)$$

where X_n is a vector containing all track-density values for the map generated with n tracks, X_{ref} is the corresponding vector for the 'reference' map (each vector with mean value μ and standard deviation σ), E is the expected value operator, and cov the covariance. This analysis was performed for a 1-mm isotropic grid-size, and the 'reference' maps were generated using 500,000 tracks (see Fig. 3). Note that the 'reference' map is subject-dependent and is different for each DWI-protocol; furthermore, by definition, $\rho(500{,}000) = 1$ for each DWI-protocol.

Directionally-encoded color (DEC) TDI maps

Analogously to the case of directionally-encoded color (DEC) maps in diffusion tensor imaging (Pajevic and Pierpaoli, 1999), fiber directionality information can be incorporated to the TDI maps. This can be done by assigning an RGB color to each spatial direction; in the case of TDI, the color in each voxel can be determined by averaging the colors of all the streamline segments contained within the voxel.

Targeted tractography

To display the connectivity network from areas visualised in the whole-brain track-density mapping, 'targeted' tracking (i.e. tracking by using seed ROIs) (Mori and van Zijl, 2002) was also performed. In particular, tracking was performed (i) from the thalamus, and (ii) from the cerebellar peduncles. These structures were selected as examples where the high-resolution track-density maps can be used to visualize brain regions not easily isolated on other images.

Thalamus

Super-resolution track-density maps with 250 μm isotropic resolution were generated using 1,000,000 tracks. Due to the high-resolution and high anatomical contrast of these maps, various sub-structures could be visually identified within the thalamus (see Figs. 1 and 2). These structures are believed to correspond to sub-thalamic nuclei. 'Targeted' fiber-tracking was performed by seeding in small ROIs positioned in thalamic structures clearly identified by visual inspection of the high-resolution track-density map.

Cerebellar peduncles

The same super-resolution track-density maps with 250 μm isotropic resolution were displayed in a coronal orientation to visualize the cerebellar peduncles. Various sub-structures were visually identified in the cerebellar peduncle region (see Fig. 6). These structures were

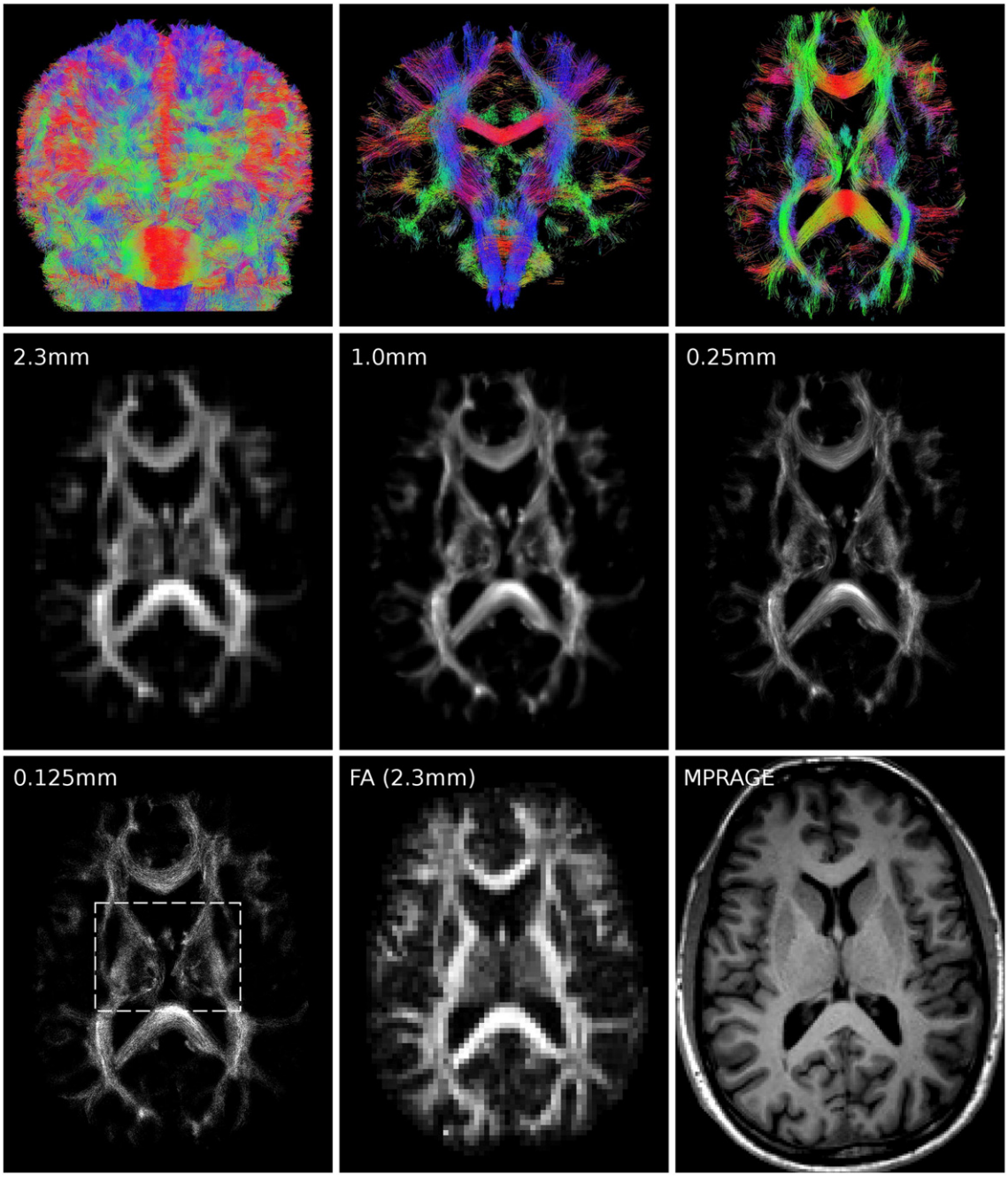

Fig. 1. Super-resolution properties of the TDI technique. Top row: whole-brain probabilistic fiber-tracking results generated from the original (low resolution) DWI data: (top-left) front-view of whole-brain; (top-middle) 2-mm coronal slab; (top-right) 2-mm axial slab. For display purposes, only 100,000 tracks are shown. The color-coding indicates the local orientation (red: left-right, green: anterior–posterior, and blue: inferior–superior). Middle row and bottom left: axial whole-brain track-density maps generated for subject *S1* with increasing spatial resolution, i.e. with decreasing grid-size: isotropic grids of 2.3 mm (the original source resolution for this subject), 1.0 mm, 250 μm and 125 μm; all TDI maps were created using 2,500,000 tracks. For comparison, FA map and the anatomical 3D T1-wighted image (MPRAGE) are also shown for the same slice locations (bottom row). The dashed region in the bottom left image shows the zoomed-area displayed in Fig. 2. To facilitate visual comparison, the TDI maps were windowed differently: the [minimum–maximum] TDI intensity range was: [0–3759] for the 2.3 mm resolution, [0–916] for the 1 mm, [0–109] for the 250 μm, and [0–34] for the 125 μm; as expected, the intensity decreases with increasing resolution (for a fixed total number of tracks).

hypothesized to correspond to the superior (SCP), middle (MCP) and inferior cerebellar peduncles (ICP). 'Targeted' fiber-tracking was performed by defining seed ROIs in these structures in the high-resolution track-density maps. Targeted probabilistic tractography was then performed (1000 tracks per seed ROI).

Results

To illustrate the super-resolution properties of this new imaging method, Fig. 1 shows axial maps generated for subject *S1* with increasing spatial resolution, i.e. with decreasing grid-size: isotropic grids of 2.3 mm (the original source resolution of the data for this subject), 1.0 mm, 250 μm, and 125 μm. For comparison, fractional anisotropy (FA) (Basser, 1995) and anatomical 3D T1-weighted images (a current state-of-the-art MRI conventional high-resolution image (MPRAGE), in this case at 1 mm isotropic resolution) are also shown for the same slice location. It should be emphasized that all track-density maps and the FA map in Fig. 1 were created using the *same* source DWI data, and the only difference is in the post-processing steps. As can be seen in the figure, whole-brain track-

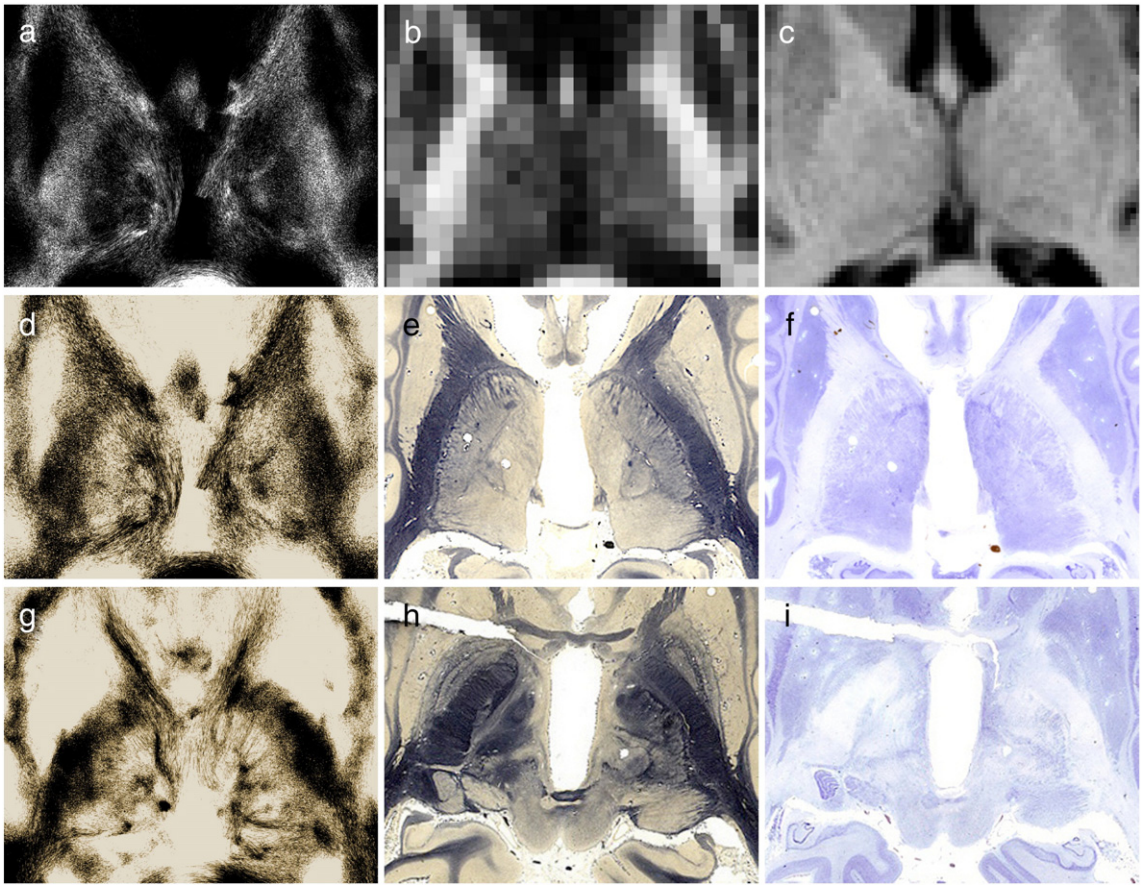

Fig. 2. Anatomical contrast and super-resolution at the level of the thalamus. Top row: zoomed-regions of axial images at the level of the thalamus (see dashed region in Fig. 1). (a) Super-resolution track-density map (for subject *S1* generated from 2,500,000 tracks with an isotropic grid-resolution of 125 μm); (b) FA map (with native resolution of 2.3 mm); (c) MPRAGE image (1 mm resolution). For qualitative comparison, the middle row shows zoomed-regions from axial histological sections from a different subject stained for myelin fibers (e) and for cells (f); these images were kindly provided by the Brain Biodiversity Bank, Michigan State University (https://www.msu.edu/~brains/brains/human/index.html), which received funding from the U.S. National Science Foundation. To help visual assessment, (d) is the same figure as (a), displayed with inverted contrast. To illustrate the complexity of the thalamic structures, the bottom row shows the corresponding data to that shown in the middle row, but for a more inferior axial slice; in this case, the track-density map (g) was generated from 6,000,000 tracks to increase the contrast-to-noise ratio, and (h) and (i) show histological sections from the Brain Biodiversity Bank (Michigan State University).

density maps show high-contrast-to-noise ratio (CNR) and very good anatomical detail, provided a sufficient number of tracks (relative to the final grid-size of the map) are generated (in all the examples shown in Fig. 1, a total of 2,500,000 tracks were used). Movie animations of TDI maps in various slice orientations can be found in the Supplementary videos 1–3 online. All these data show that whole-brain track-density maps can be used to create very high-quality, high-resolution images of brain white matter, despite coarse resolution source DWI data, thus achieving super-resolution. The figure also illustrates the unique anatomical contrast contained in these images, providing detail and contrast not achievable by other MRI modalities.

To illustrate the extremely high-resolution of these maps, Fig. 2 shows a zoomed-region of an axial track-density map at the level of the thalamus, generated with an isotropic grid-resolution of 125 μm. Once again, for comparison, the zoomed-regions on the FA map and MPRAGE image are shown. The new super-resolution TDI method allows a massive increase in the spatial resolution achievable with MRI, providing fine anatomical information not previously available *in vivo*. Note that the image pixels in the new method are so small that they cannot be discerned in the zoomed-region of the figure (left). For qualitative comparison, the middle and bottom rows show zoomed-regions from axial histological sections stained for myelin fibers and for cells (NB. from a different individual). While the TDI method highlights white matter tracts in structures such as the thalamus where intrinsic contrast is poor, this creates a novel contrast that allows visualization of the many individual nuclei that make up the thalamus (Figs. 2d and g).

The trade-off between number of tracks used to generate the track-density maps and the quality of the map (for a fixed grid-size) is illustrated in Fig. 3. This figure shows the correlation ρ as a function of the number of tracks (each curve corresponds to a subject acquired with one of the DWI-protocols, i.e. subjects *S1*/*S4*/*S5* for the 150/60/20 DWI direction protocols, respectively). As shown in the figure, for a given quality (i.e. a given correlation value), a smaller number of tracks are required when using data acquired with more DWI-directions (and analyzed with an appropriate *lmax*). An example of the improvement in image quality with increasing number of tracks is also shown in the figure, for the data acquired from subjects *S1* and *S5*. As can be appreciated from the maps, their CNR improve with increasing number of tracks, particularly in the range of 10,000–150,000 tracks (for the 1 mm isotropic grid-size used in this figure). Similar qualitative trends were observed for other grid-sizes (data not shown).

Fig. 4 shows an illustration of directionality information incorporated into the TDI maps. As can be appreciated in the figure, these color maps retain the super-resolution properties of the TDI method, thus producing super-resolution DEC TDI maps. However, it should be noted that the color-encoding can actually detracts from the detailed anatomical information available in the TDI maps, and the color could therefore potential hinder the assessment of biologically meaningful white matter structures.

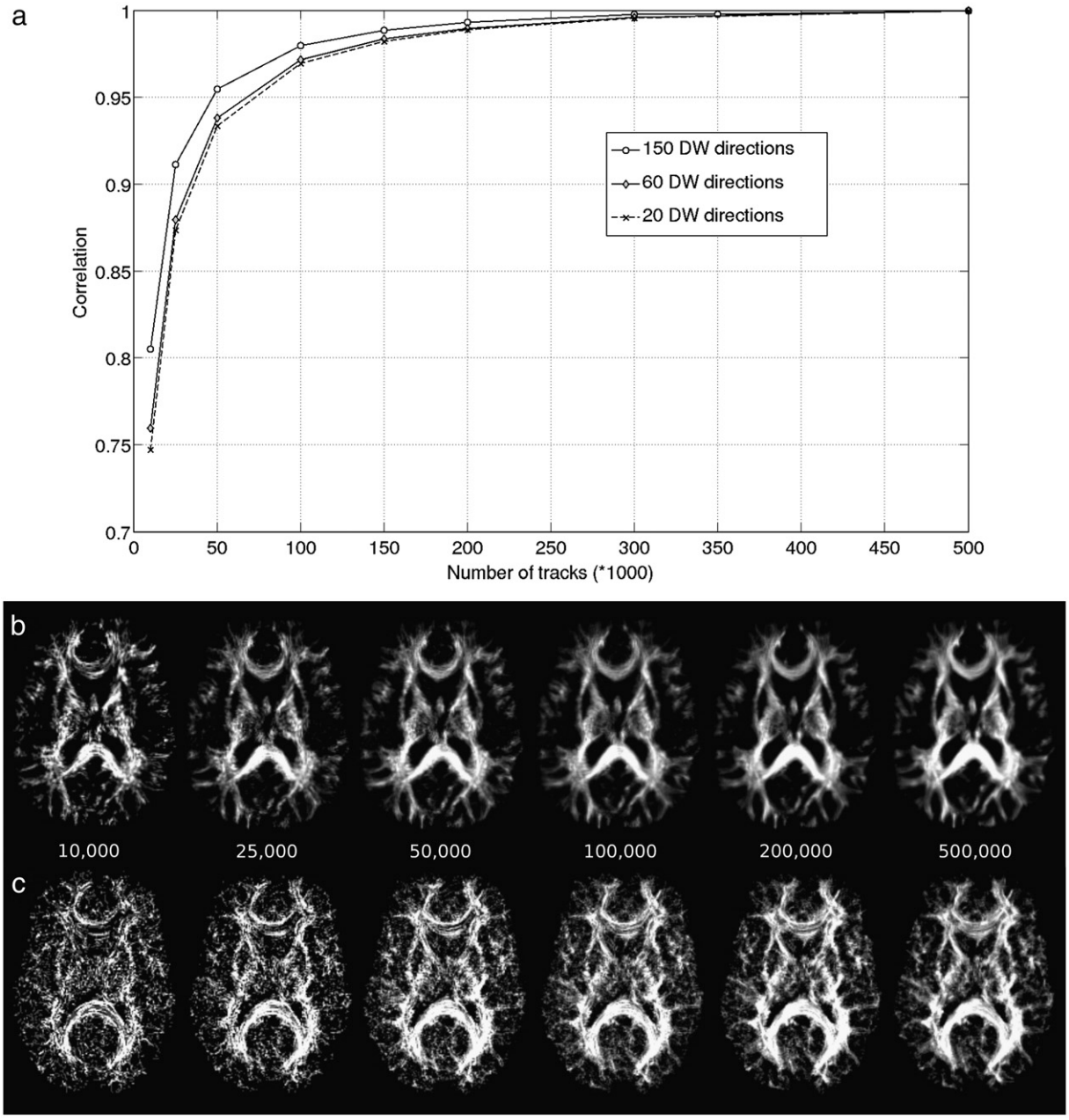

Fig. 3. Effect of number of tracks on track-density map quality. (a) Correlation between a 'reference' track-density map (from 500,000 tracks) and maps generated with a subset of tracks (NB. Each DWI-protocol has its own 'reference' map). Results are shown for subjects *S1*/*S4*/*S5* (for the 150/60/20 DWI direction protocols, respectively); a 1 mm isotropic grid-size was used for all cases. For a given quality (i.e. correlation value), a smaller number of tracks are required with more DWI-directions. (b) Axial maps (1 mm isotropic resolution) of the data from subject *S1*, generated with increasing number of tracks; (c) corresponding data from subject *S5*. For each DWI-protocol, the CNR on the maps improves with increasing number of tracks, but the 150-direction protocol used in *S1* always gives superior CNR than the 20-direction of *S5*.

The high-contrast of the super-resolution maps enables highly-specific fiber-tracking analysis. For example, Fig. 5 shows the various connections from small seed ROIs defined in structures identified in the super-resolution TDI maps at the level of the thalamus. It can be seen that the anterior–posterior distribution of seed ROIs in the thalamus reflects projections in a similar anterior–posterior order throughout the fronto-parietal cortex. This high degree of organization in the thalamo-cortical tract projections argues strongly for the intrinsic reality of the thalamic contrast that allowed precise placement of the seeds in sub-thalamic fasciculi.

Fig. 6 shows an example of the ability of these high-quality track-density maps to directly visualize the various cerebellar peduncles. Three distinct white matter regions can be seen in an area of the cerebellar peduncle (see arrows in (b)), which correspond to the SCP, MCP and ICP. These 3 structures are not apparent in either the conventional high-resolution MRI (Fig. 6e) or the FA map (Fig. 6d). To corroborate these assignments, the maps were used to define a separate seed ROI in each of these three structures (Fig. 6b) in order to perform 'targeted' fiber-tracking (probabilistic tractography with 1000 tracks per seed ROI). As can be seen in the tracking results (Figs. 6f–i), the various connections are consistent with the known anatomical connections of the three cerebellar peduncles.

As an illustration of the consistency of structures identified by super-resolution TDI, Fig. 7 shows tilted-axial slices including the connections between the cerebellum, the thalamus and the frontal lobes for the 3 subjects scanned with the 150 DWI-protocol. The figure shows the power of super-resolution TDI for displaying the white matter pathways that connect critical structures in the brain.

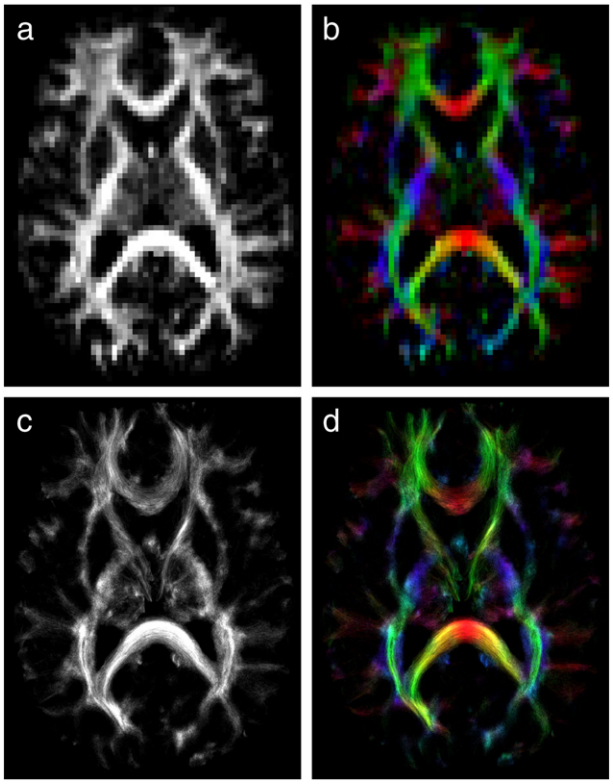

Fig. 4. Directionally-encoded color (DEC) maps from subject *S1*. (a) FA map, and (b) DEC map; both maps were calculated based on the tensor model, with native 2.3 mm isotropic resolution. (c) Super-resolution TDI map, and (d) super-resolution DEC TDI map; both maps were generated using 1 million tracks and a 250 μm isotropic grid. The color-coding indicates the main local orientation (red: left-right, green: anterior–posterior, blue: inferior–superior), defined based on the tensor model (for (b)) or on the streamlines contained in the grid element (for (d)).

Combined with this imaging plane, we can appreciate how the white matter tracts from the cerebellum pass to the thalamus. The cerebellum is often not considered in brain and mind disorders that involve frontal and temporal connections, but these images demonstrate critical structural connections that could complement fiber-tracking and functional-connectivity studies in human disease.

Discussion

This study has shown that the novel super-resolution TDI technique provides a method to produce high-quality white matter images, with high spatial resolution, and exquisite anatomical contrast not achievable with other MRI modalities. A unique property of these maps is their super-resolution nature: their spatial resolution and SNR can be tailored depending on the chosen grid-size and the total number of tracks generated. For example, Fig. 2 showed that high-quality 125 μm isotropic resolution maps can be generated from 2.3 mm source DWI data, i.e. an image with ~6000 times smaller voxel size. This gain in resolution should not be confused with the visual effect achieved using standard image interpolation: interpolation does not provide any extra information and it has mainly a 'cosmetic' role. This distinction is illustrated in Fig. 8, where the super-resolution TDI map is compared with the corresponding standard interpolated map.

Although the whole-brain TDI maps are generated from traditional DWI data, they can provide higher anatomical resolution than commonly used diffusion anisotropy maps (e.g. FA map) (Basser, 1995). The latter suffer from a 'dilution' effect (given by the partial-volume-effect of the acquired coarse DWI data) that cannot be overcome by image interpolation; these commonly used diffusion scalar maps only provide *whole-voxel average* information, which cannot then be disentangled to achieve super-resolution. In contrast, the practical resolution of the track-density maps is determined by the track information in the whole neighborhood: since tracks shorter than a user defined length (10 mm in our study) are discarded, only tracks that are consistent with the local neighborhood on at least that scale will contribute to the track-density value in each grid element. It is the information content from the very large number of streamlines (each generated with a small step-size) that allows the gain in spatial resolution in the final track-density maps. The simplest example as illustration of this effect is at the interface between white matter and cerebrospinal fluid (CSF); this is illustrated in the schematic example shown in Fig. 9, where the lack of fiber-tracks originating from the CSF area can be used to produce a sharper delineation of the interface between the tissue structures.

Super-resolution imaging

The main principle behind the super-resolution properties of TDI can be understood in simple terms as follows: while the brain itself is a continuous object, the source MRI data only provide a *discrete* representation (i.e. discretized by the acquired voxels). By generating a very large number of fiber-tracks, one can however create a *continuous* representation of the brain (given by the fiber-tracking model). Once this continuous model is generated, the original discrete representation of the brain (i.e. the acquired image) is irrelevant, and the new continuous representation can then be discretized to a resolution much finer than the original image resolution, thus achieving significantly improved resolution.

MRI has revolutionized the diagnosis, understanding, and management of many diseases, as well as contributed immensely to neurosciences research. However, MRI suffers from an intrinsic limitation: the spatial resolution, the SNR, and the acquisition time of the images are strongly coupled. With current MRI methods, this interdependency makes it impossible to improve any of these aspects without compromising the others (Kale et al., 2009). The technique of super-resolution TDI introduced here can achieve higher spatial resolution than what was previously possible using *in vivo* MRI in the human brain (Duyn et al., 2007). Importantly, for a given MRI data-set (i.e. for a fixed number of DW directions) this higher resolution can be achieved not at the expense of SNR or by an associated increased acquisition time.

It should be emphasized that acquiring MRI images with such high spatial resolution is usually associated with very low SNR (or alternatively, they require impractically long acquisition times). Recent advances in ultra-high field MRI (7 T and above) have allowed very high-resolution imaging (Duyn et al., 2007). These images have provided outstanding image contrast (both for grey matter and white matter) and spatial resolution (achievable resolution ~$240\times240\times1000\ \mu m^3$) (Duyn et al., 2007). This spatial resolution is beyond the practical limits at more commonly used field strengths (1.5–3 T). The super-resolution TDI method provides a means for achieving comparable resolution, even at such lower field strengths (e.g. see $125\times125\times125\ \mu m^3$ in Fig. 2). In addition, full brain coverage is not a limitation for super-resolution TDI (NB. to obtain full brain coverage data at 125 μm-resolution by MRI acquisition requires almost 1000 slices, which is unfeasible in practice at any field strength). Therefore, super-resolution TDI provides a very powerful additional imaging modality for the study of brain white matter, and provides a novel contrast mechanism in tissues of mixed grey and white matter, even at more commonly available magnetic field strengths.

Other super-resolution methods have been previously used in MRI, including some controversial work in diffusion MRI (Peled and Yeshurun, 2001; Scheffler, 2002; Peled and Yeshurun, 2002). These methods use the more standard super-resolution principle of combining multiple images acquired with relative sub-voxel shifts.

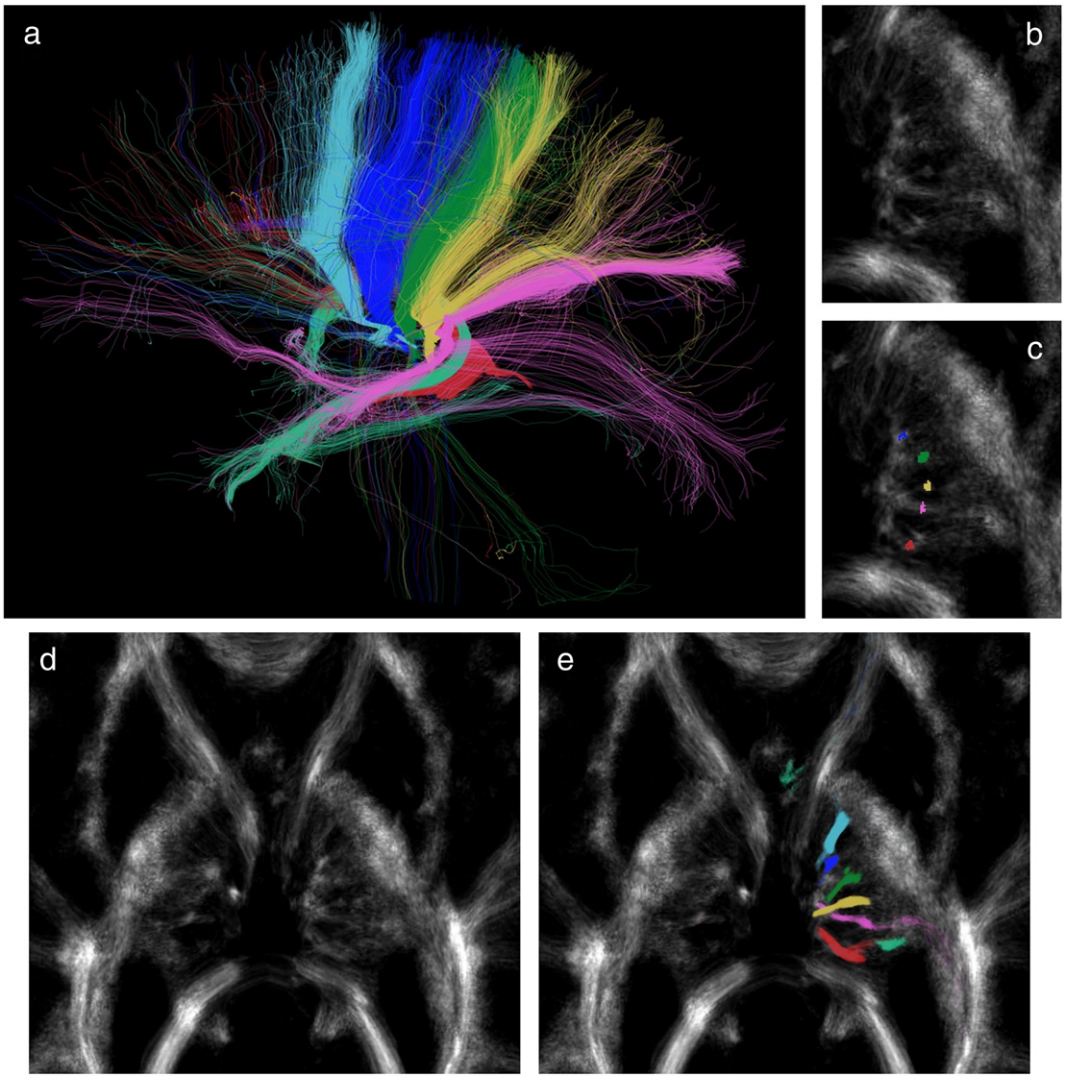

Fig. 5. Targeted fiber-tracking for seeds defined in the thalamus. (a) Targeted fiber-tracking resulting from 7 small seed ROIs. The tracks are shown on a sagittal projection (left side of image is anterior anatomically), and the tracks generated from each seed ROI are labeled with different colors. The seed ROIs were defined in areas identified in the high-contrast TDI maps (maps generated with 250 μm isotropic resolution using 1,000,000 tracks); see (b) for an example axial slice (zoomed at the level of the thalamus), and (c) for 5 of the 7 seed ROIs present in that slice (the remaining 2 seed ROIs were defined in different slices). (d) Zoomed-region on a different axial slice at the level of the thalamus, and (e) the corresponding fiber-tracking results (only the tracks within the 250 μm-slice are displayed). The color-coding used in (c) and (e) corresponds to the same convention used in (a). Note that the fiber-tracking results are generated from the original (low resolution) DWI data, and the TDI maps are only used to define the seed ROIs.

The use of multiple shifted images has also been exploited for super-resolution in many other imaging modalities, including video and satellite imaging. In the context of standard 2D MRI, it is now generally accepted that this approach can only lead to super-resolution in the slice-encoded direction due to the band-limited nature of Fourier-encoded data (Greenspan et al., 2002). While the super-resolution approach proposed here also relies on increasing resolution by combining information from multiple images (i.e. using the fiber-tracking model generated from those images), it is based on a different principle to the standard super-resolution method (i.e. the images used to construct the TDI maps are not shifted relative to each other, but use additional information provided by the continuous nature of the long-range fiber-tracks).

Technical considerations

While fiber-tracking studies can require significant user interaction (and therefore a potential source of subjectivity and variability) the TDI method described here relies on *whole-brain* tracking, where no seed/target regions need to be defined. The procedure can therefore be implemented in a fully automatic and completely objective way. This should facilitate their widespread use since their production does not rely on the presence of specialized trained staff locally.

The step-size of the streamlines algorithm should be smaller than the dimensions of the grid-size of the final TDI map. It is for this reason that a relatively small step-size (i.e. 0.1 mm) was used in this study. One of the drawbacks of this requirement is an increase in processing time for the tractography step; however, this can be ameliorated by multi-threaded processing. As an indication of the processing time involved, using the *MRtrix* software on a standard desktop workstation (Intel Core2 Quad 2.8 GHz, 4Gb RAM, 64-bit Linux), the steps involved in generating a typical TDI map (1 million tracks and 250 μm isotropic resolution) can be performed in: 2 min for the CSD analysis, 50 min for generating the tracks, and 2 min to generate the TDI map.

It should be emphasized that increasing the number of fiber-tracks in post-processing cannot compensate for the use of a protocol with small number of DWI-directions during acquisition. For example, the TDI maps generated from the 20 DWI-protocol in this study will not have the same quality as those generated from the 150 DWI-protocol,

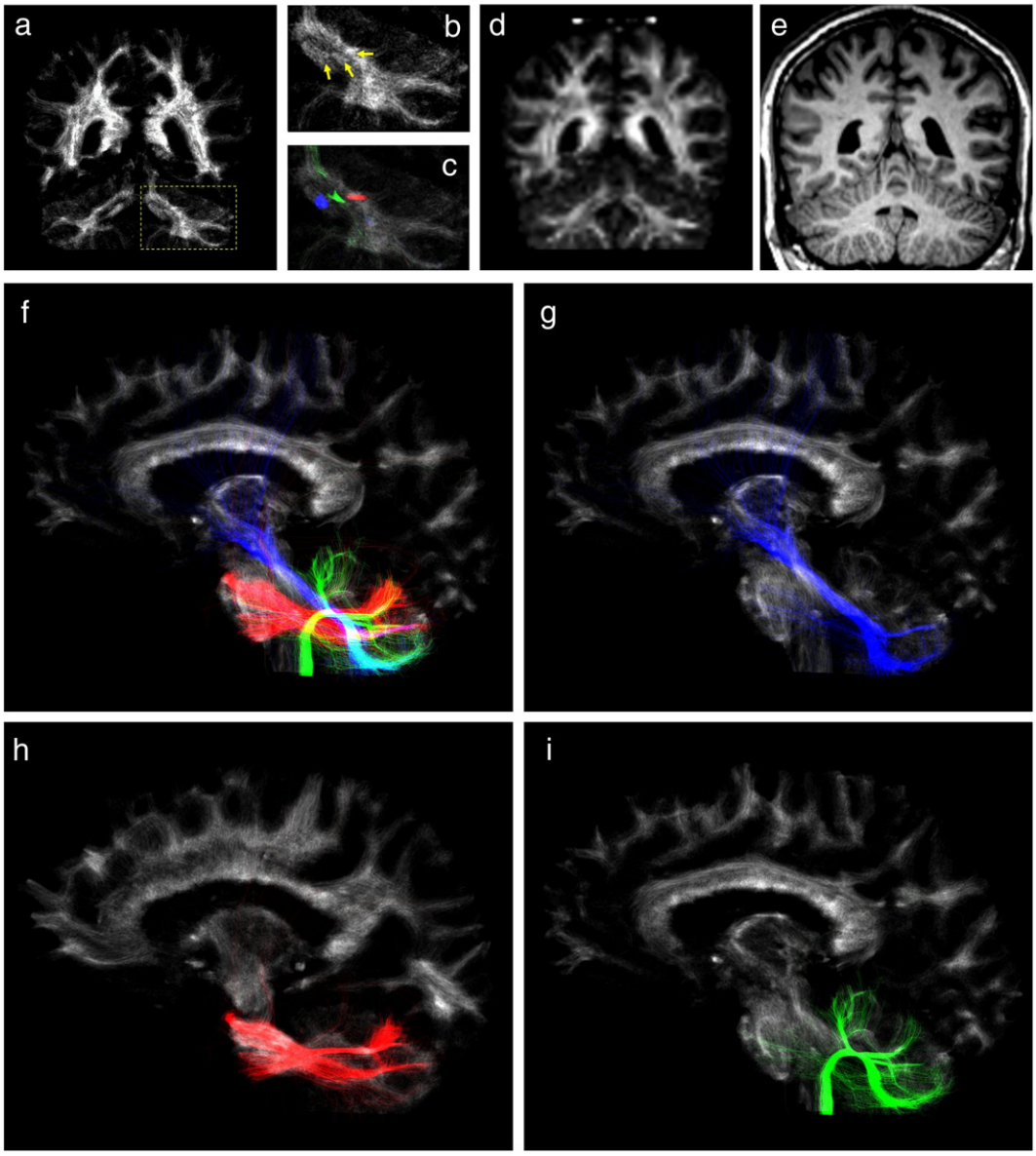

Fig. 6. TDI example of the cerebellar peduncles. (a) Coronal whole-brain track-density map (1,500,000 tracks, 250 μm isotropic grid) from subject *S1*. (b) Zoomed-image of the region highlighted in (a): 3 distinct white matter regions can be seen (see arrows), which correspond to the superior (SCP), middle (MCP) and inferior cerebellar peduncles (ICP). Three separate seed regions were positioned in these 3 structures, and probabilistic tractography was then performed (1000 tracks/seed ROI). (c) Zoomed-region with the tracks overlaid (blue: SCP, red: MCP, green: ICP; only tracks within a 2-mm slab are shown). (d) Corresponding coronal FA map (interpolated to 1 mm isotropic resolution). (e) Corresponding coronal MPRAGE. Note the lower contrast and insufficient demarcation of the various cerebellar peduncles in the FA map and MPRAGE image. (f) Sagittal whole-brain track-density map with the results of the seeded fiber-tracking superimposed (blue: SCP, red: MCP, green: ICP). For clarity, the three different results are separately shown in figures (g), (h), and (i) for the SCP, MCP, and ICP, respectively. Note that the fiber-tracking results are generated from the original (low resolution) DWI data, and the TDI maps are only used to define the seed ROIs.

regardless of the number of fiber-tracks used when creating the TDI map for the 20 DWI data-set (see for example maps in Fig. 3). This is due to the need of a sufficient number of DWI-directions and SNR in order to reduce the uncertainty in defining the white matter fiber directions and to have sufficient angular resolution to resolve areas of 'crossing-fibers' (Tournier et al., 2007). Therefore, the TDI method benefits from the use of so-called high angular resolution diffusion imaging (HARDI) data (Tuch et al., 2002). Similarly, while lower *b*-values such as those typically used in clinical studies ($b = 1000$ s/mm^2) are able to resolve multiple fiber-orientations (Behrens et al., 2007; Tournier et al., 2007), higher *b*-values ($b \sim 3000$ s/mm^2) have been shown to be beneficial due to the increase in angular resolution for resolving crossing-fibers. Therefore, the TDI method will also benefit from the use of high *b*-values.

The underlying assumption of the proposed method is that white matter connections in the brain are long-range, and that fiber-tracking methods can provide a suitable representation of these connections in a continuous and smooth manner. It is important to note that the super-resolution method described here does not rely on the fiber-tracking algorithm inferring the correct anatomical connectivity between brain areas. It does however rely on the algorithm identifying the correct *location* for the underlying fiber bundles; that is, the particular brain areas those bundles connect will only have an effect on the relative intensity of the TDI map, without affecting the delineation of the boundaries between structures (i.e. its super-resolution properties). In this context, it is essential to use a diffusion MRI model that accounts for the presence of multiple-fiber populations within a voxel: if the tensor model is used, the errors introduced

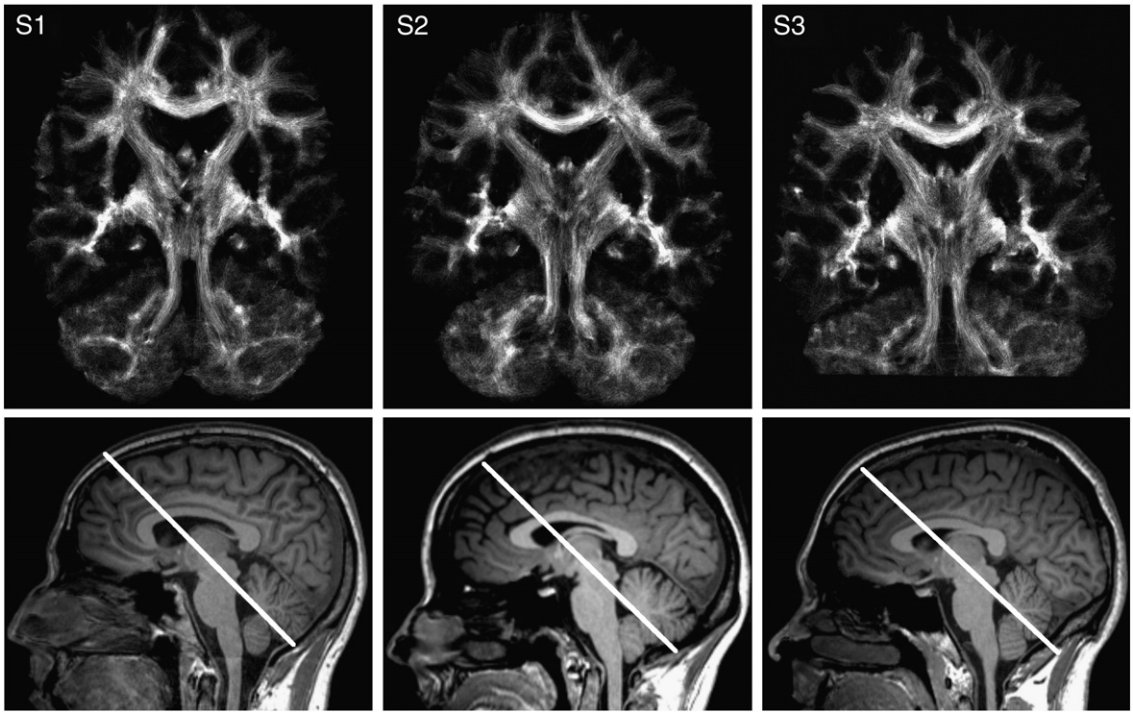

Fig. 7. Top row: example TDI maps of tilted-axial slices (as indicated in the corresponding bottom row images) including the cerebellum, the thalamus and the frontal and temporal lobes for subjects *S1* (left), *S2* (middle), and *S3* (right). All TDI maps were generated with 250-μm isotropic resolution using 2,500,000 tracks. Direct visualization of white matter structures can be observed in all subjects. We have chosen this image because it demonstrated in a novel way the convergence of white matter tracts from the frontal lobe (anterior bundle), temporal lobe (middle bundle) and cerebellum (posterior bundle) on the thalamus and sub-cortical structures.

during tracking artificially enhance certain white matter regions. In this study, we used the CSD method (Tournier et al., 2007) and the probabilistic streamlines algorithm; however, other methods to resolve crossing-fibers (Seunarine and Alexander, 2009) could be used instead. Furthermore, the field of fiber-tracking MRI is a fast-developing and active field; any future developments in fiber-tracking algorithms can be incorporated into the calculation of the TDI maps. Therefore, the TDI approach should benefit from more sophisticated tracking algorithms; for example, more recent global-based tractography methods (Jbabdi et al., 2007) could be used to improve the delineation of white matter structures by incorporating information beyond the local neighborhood.

Direct visualization of brain sub-structures

The high-quality images obtained using TDI enable direct visualization of brain sub-structures that, as shown by the targeted fiber-tracking results (Figs. 5 and 6), have different structural connectivity characteristics. For example, state-of-the-art high-resolution conventional MRI (Fig. 6e) shows the three cerebellar peduncles as a continuum. In contrast, the TDI maps enable differentiation of the ICP, MCP and SCP, as evidenced by their separately delineated structural connections.

Future validation studies are needed to ensure the veracity of the sub-structures visualised by TDI in the thalamus. However, these structures have striking similarities to those found (on a different subject) on histological sections stained for myelin (Fig. 2). The myelin sections included in Fig. 2 show high levels of myelin in well-localised thalamic regions; we hypothesize that these are the regions visualised in the TDI maps. Future studies are needed to test this hypothesis.

Complementary tool for tractography studies

The TDI technique not only has a role in structural delineation of brain features (due to its high anatomical contrast), but can also play a very important complementary role in tractography studies. The TDI maps provide an ideal tool for guiding seed/target ROI definition in tractography investigations: provided a very large number of tracks are used to generate the maps (of the order of several hundred thousands to millions), the TDI maps can be used to delineate the specific regions in which tracks are expected to be present. Importantly, since the TDI maps

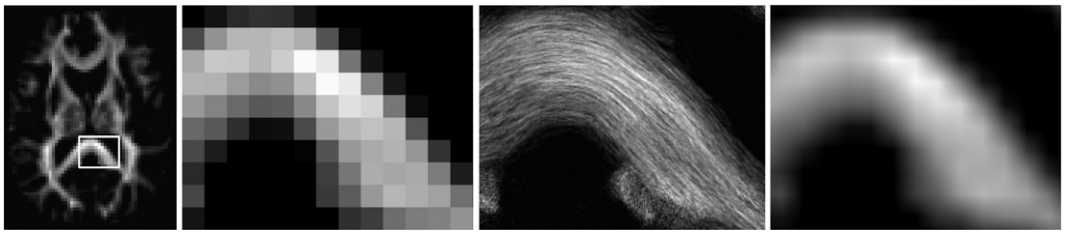

Fig. 8. Comparison of the effect of super-resolution vs. the standard image interpolation for subject *S1*. (a) Axial TDI map (2.3 mm resolution); a zoomed version of the highlighted white-box is shown (b). (c) Corresponding super-resolution version (125 μm resolution) of the zoomed-region. (d) Standard linear interpolation of the image shown in (b). The major improvement in spatial resolution achieved with the super-resolution method is easily observed: the super-resolution method allows the real anatomy of fibers in the image plane and passing through it (the bundle inferior to the forceps major) to be easily distinguished; this is not possible in the interpolated image.

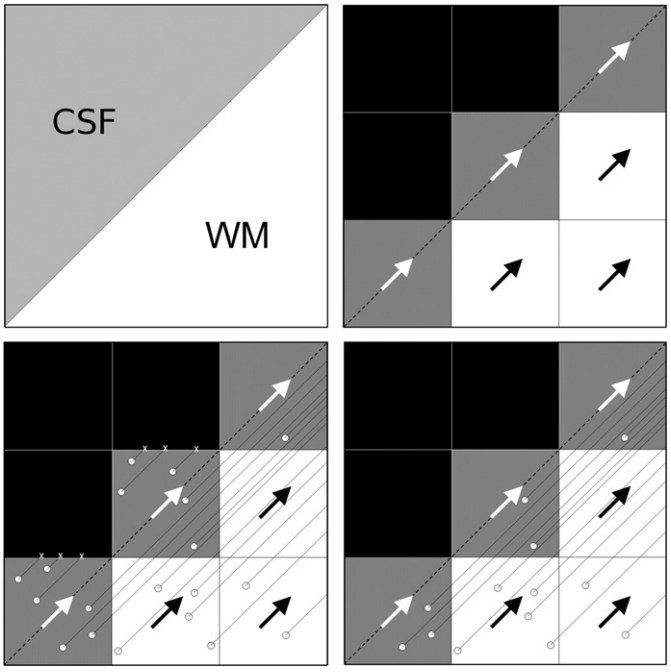

Fig. 9. Schematic figure to illustrate the potential higher anatomical contrast definition in the track-density maps compared to fractional anisotropy maps (FA). Top left: schematic region with interface between cerebrospinal fluid (CSF) and white matter (WM). Top right: 3×3 voxel region in the interface; the grey scale represents the FA value in the voxel, the arrows the direction of the white matter fibers, and the dashed line the CSF–WM interface. Bottom left: schematic diagram of tracking results: streamlines were started from the white circles; the white crosses indicate track termination; note that no streamlines arrive to the WM area from the CSF voxels. Bottom right: Since tracks shorter than a user defined threshold are discarded, the CSF–WM interface can be characterized more accurately by calculating the resulting track-density in each element of a finer grid (grid not shown in the figure). By generating a sufficient number of such tracks, the white matter area would be filled appropriately.

are created from the tracks themselves, they are in *exactly* the same space (including the spatial image distortions of the MRI acquisition) as the diffusion data (unlike the commonly used high-resolution 3D T1-weighted images). Therefore, similar precise placement of seed ROIs would not be feasible by using conventional high-resolution images.

Further potential use of TDI

Due to their high anatomical information and white matter specificity, the whole-brain TDI maps could be used as scalar maps to detect *structural* differences in group comparisons, using methods such as voxel-based morphometry (VBM) (Ashburner and Friston, 2000). Furthermore, if the pixel intensity values in the maps were shown to have good quantitative reproducibility, the intensity values themselves could also be used as an alternative to anisotropy maps (e.g. FA maps) in quantitative voxel-based analysis (VBA) (Smith et al., 2006; Jones et al., 2005; Embleton et al., 2007). Since the pixel intensity value in the track-density map is determined by the total number of tracks traversing a given grid element, two situations could lead to an abnormality in the map, and therefore a potential group difference in voxel-based methods: first, a white matter abnormality in that grid element; second, an abnormal number of tracks connecting to that grid element (e.g. due to a remote abnormality in an area that would have been connected otherwise, or the presence of extra connections to that grid element). A region of abnormality identified in the map could therefore be used as a seed ROI for subsequent fiber-tracking analysis, thus identifying the brain regions that have contributed to its track-density value. By comparing these results with those in normal situations (e.g. in normal subjects, or in the contralateral side), the areas responsible for the abnormality could be identified. Further work is required to assess the role of the track-density maps in voxel-based methods.

The high-contrast and super-resolution qualities of the maps make them also a good candidate as a scalar image for use in inter-subject normalization of tractography results: the transformation obtained after non-linear normalization of the TDI maps could be applied to the individual coordinates of the fiber-tracking results, thus transforming the fiber-tracks to a common space for subsequent inter-subject comparisons (Calamante et al., 2009).

In conclusion, whole-brain super-resolution TDI maps should play an important role in neurology and neurosciences studies, as they provide exquisite anatomical information with high SNR and a novel contrast mechanism for tissues of mixed grey matter and white matter. This approach constitutes a major new advance in technology for the study of white matter in the human brain and its role in human diseases. Not only does TDI provide super-resolution anatomical data, but it can also be a very valuable complementary tool for white matter fiber-tracking studies.

Acknowledgments

We are grateful to the National Health and Medical Research Council (NHMRC) of Australia and the Austin Health for the support. We thank Dr. Heath Pardoe (Brain Research Institute, Australia) for the helpful discussions, and Mr. Robert E. Smith (Brain Research Institute, Australia) for his help in implementing the directionally-color encoded TDI maps.

Appendix A. Supplementary data

Supplementary data associated with this article can be found, in the online version, at doi:10.1016/j.neuroimage.2010.07.024.

References

Ashburner, J., Friston, K.J., 2000. Voxel-based morphometry: the methods. Neuroimage 11, 805–821.
Bandettini, P.A., 2009. What's new in neuroimaging methods? Ann. NY Acad. Sci. 1156, 260–293.
Basser, P.J., 1995. Inferring microstructural features and the physiological state of tissues from diffusion-weighted images. NMR Biomed. 8, 333–344.
Behrens, T.E., Johansen-Berg, H., Woolrich, M.W., Smith, S.M., Wheeler-Kingshott, C.A., Boulby, P.A., Barker, G.J., Sillery, E.L., Sheehan, K., Ciccarelli, O., Thompson, A.J., Brady, J.M., Matthews, P.M., 2003. Non-invasive mapping of connections between human thalamus and cortex using diffusion imaging. Nature Neurosci. 6, 750–757.
Behrens, T.E., Berg, H.J., Jbabdi, S., Rushworth, M.F., Woolrich, M.W., 2007. Probabilistic diffusion tractography with multiple fibre orientations: what can we gain? Neuroimage 34, 144–155.
Calamante, F., Tourneir, J.D., Pardoe, H., Connelly, A., 2009. Whole-brain track-density mapping as a tool for fiber tractography. Proc. 17th Annual Meeting of the Int. Soc. Magn. Reson. Med (ISMRM), Honolulu, USA, vol. 17, p. 1442.
Duyn, J.H., van Gelderen, P., Li, T.Q., de Zwart, J.A., Koretsky, A.P., Fukunaga, M., 2007. High-field MRI of brain cortical substructure based on signal phase. Proc. Natl Acad. Sci. USA 104, 11796–11801.
Embleton, K.V., Morris, D.M., Haroon, H.A., Lambon Ralph, M.A., Parker, G.J., 2007. Anatomical connectivity mapping. Proc. 15th Annual Meeting of the Int. Soc. Magn. Reson. Med (ISMRM), Berlin, Germany, vol. 15, p. 1548.
Gillard, J.H., Waldman, A.D., Barker, P.B. (Eds.), 2005. Clinical MR Neuroimaging: Diffusion, Perfusion and Spectroscopy. Cambridge University Press, Cambridge, UK.
Greenspan, H., Oz, G., Kiryati, N., Peled, S., 2002. MRI inter-slice reconstruction using super resolution. Magn. Reson. Imaging 20, 437–446.
Jbabdi, S., Woolrich, M.W., Andersson, J.L., Behrens, T.E., 2007. A Bayesian framework for global tractography. Neuroimage 37, 116–129.
Jones, D.K., Symms, M.R., Cercignani, M., Howard, R.J., 2005. The effect of filter size on VBM analyses of DT-MRI data. Neuroimage 26, 546–554.
Kale, S.C., Chen, X.J., Henkelman, R.M., 2009. Trading off SNR and resolution in MR images. NMR Biomed. 22, 488–494.
Kwong, K.K., Belliveau, J.W., Chesler, D.A., Goldberg, I.E., Weisskoff, R.M., Poncelet, B.P., Kennedy, D.N., Hoppel, B.E., Cohen, M.S., Turner, R., et al., 1992. Dynamic magnetic resonance imaging of human brain activity during primary sensory stimulation. Proc. Natl Acad. Sci. USA 89, 5675–5679.
Matthews, P.M., Honey, G.D., Bullmore, E.T., 2006. Applications of fMRI in translational medicine and clinical practice. Nat. Rev. Neurosci. 7, 732–744.
Mori, S., van Zijl, P.C., 2002. Fiber tracking: principles and strategies — a technical review. NMR Biomed. 15, 468–480.

Moseley, M.E., Cohen, Y., Mintorovitch, J., Chileuitt, L., Shimizu, H., Kucharczyk, J., Wendland, M.F., Weinstein, P.R., 1990. Early detection of regional cerebral ischemia in cats: comparison of diffusion- and T2-weighted MRI and spectroscopy. Magn. Reson. Med. 14, 330–346.

Pajevic, S., Pierpaoli, C., 1999. Color schemes to represent the orientation of anisotropic tissues from diffusion tensor data: application to white matter fiber tract mapping in the human brain. Magn. Reson. Med. 42, 526–540.

Parker, G.J., Alexander, D.C., 2005. Probabilistic anatomical connectivity derived from the microscopic persistent angular structure of cerebral tissue. Philos. Trans. R. Soc. B 360, 893–902.

Peled, S., Yeshurun, Y., 2001. Superresolution in MRI: application to human white matter fiber tract visualization by diffusion tensor imaging. Magn. Reson. Med. 45, 29–35.

Peled, S., Yeshurun, Y., 2002. Superresolution in MRI — perhaps sometimes. Magn. Reson. Med. 48, 409-409.

Reese, T.G., Heid, O., Weisskoff, R.M., Wedeen, V.J., 2003. Reduction of eddy-current-induced distortion in diffusion MRI using a twice-refocused spin echo. Magn. Reson. Med. 49, 177–182.

Scheffler, K., 2002. Superresolution in MRI? Magn. Reson. Med. 48, 408-408.

Seunarine, K.K., Alexander, D.C., 2009. Multiple fibres: beyond the diffusion tensor. In: Behrens, T.E., Johansen-Berg, H. (Eds.), Diffusion MRI. Elsevier.

Smith, S.M., Jenkinson, M., Johansen-Berg, H., Rueckert, D., Nichols, T.E., Mackay, C.E., Watkins, K.E., Ciccarelli, O., Cader, M.Z., Matthews, P.M., Behrens, T.E., 2006. Tract-based spatial statistics: voxelwise analysis of multi-subject diffusion data. Neuroimage 31, 1487–1505.

Thomas, D.L., Lythgoe, M.F., Pell, G.S., Calamante, F., Ordidge, R.J., 2000. The measurement of diffusion and perfusion in biological systems using magnetic resonance imaging. Phys. Med. Biol. 45, R97–R138.

Tournier, J.D., Calamante, F., Gadian, D.G., Connelly, A., 2004. Direct estimation of the fibre orientation density function from diffusion-weighted MRI data using spherical deconvolution. Neuroimage 23, 1176–1185.

Tournier, J.D., Calamante, F., Connelly, A., 2007. Robust determination of the fibre orientation distribution in diffusion MRI: non-negativity constrained super-resolved spherical deconvolution. Neuroimage 35, 1459–1472.

Tuch, D.S., Reese, T.G., Wiegell, M.R., Makris, N., Belliveau, J.W., Wedeen, V.J., 2002. High angular resolution diffusion imaging reveals intravoxel white matter fiber heterogeneity. Magn. Reson. Med. 48, 577–582.